

Inter-turn Short-circuit Fault Diagnosis and Severity Estimation for Five-phase PMSM

Yijia Huang, Wentao Huang, *Member, IEEE*, Tinglong Pan, and Dezhi Xu, *Senior Member, IEEE*

Abstract—In this article, an inter-turn short-circuit (ITSC) fault diagnosis and severity estimation method based on extended state observer (ESO) and convolutional neural network (CNN) is proposed for five-phase permanent magnet synchronous motor (PMSM) drives. The relationship between fault parameters and motor parameters is analyzed and the equivalent model of ITSC faults in the natural reference frame is accordingly derived. To achieve fault detection and location, the short-circuit turn ratio and short-circuit current are integrated as the fault diagnosis index. According to the model of the short-circuit current, an ESO is designed for the estimation of the fault diagnosis index. Further, the sensitivity analysis among fault parameters is conducted to evaluate the short-circuit turn ratio and the short-circuit resistance. Subsequently, the postfault current, back electromotive force, electrical angular velocity, q_1 -axis current reference and the fault diagnosis index are selected as the input signals of CNN to estimate the short-circuit turn ratio. This approach not only resolves parameter coupling challenges but also provides a quantitative assessment of fault severity. Finally, simulations and experiments under different operating points validate the effectiveness of the proposed method.

Index Terms—Multi-phase drive, Permanent magnet synchronous motor, Inter-turn short-circuit, Fault diagnosis.

I. INTRODUCTION

RECENTLY, multiphase permanent magnet synchronous motors (PMSMs) have become the preferred solution for high-reliability electromechanical systems, primarily attributed to their advantages of higher power density and enhanced fault-tolerant ability over three-phase PMSMs [1]-[3]. Meanwhile, with the growing emphasis on reliability and safety in motor drive systems, substantial research has been made toward advanced fault diagnosis and fault-tolerant control [4]-[7].

Winding insulation failure ranks among the most frequent motor malfunctions, accounting for 30%–40% of all motor

failure cases. Notably, inter-turn short-circuit (ITSC) faults constitute a considerable proportion [8]-[9]. Generally, ITSC faults originate in winding faults owing to thermal, electrical, and mechanical stress [10]. Especially for PMSMs, the magnetic field generated by ITSC faults is usually stronger than the coercivity of the magnet, which may lead to irreversible demagnetization [11]. In addition, a large current circulating in the short-circuit loop would result in a severe temperature rise, accelerating the aging and embrittlement of insulation materials. If not handled in time, an ITSC fault may cause an entire winding failure and even endanger personal safety [12]. Therefore, the detection and location of ITSC faults at the early stage have emerged as a critical topic for improving the reliability of PMSM drive systems [13].

Existing research for ITSC fault diagnosis of PMSMs can be mainly divided into three categories: signal-based methods, model-based methods and artificial intelligence (AI)-based methods [14]-[15].

Most of the signal-based methods depend on stator current signals, including fundamental components, zero-sequence components and negative-sequence components [12]. As these methods rely on the amplitudes of stator currents, they may cause false alarms under low-load conditions. Spectrum analysis, such as fast Fourier transformation (FFT) [16], wavelet transformation [17], and Hilbert-Huang transformation [18], is used for extracting certain sequences of signals. Nevertheless, these methods require a batch of samples to analyze signals, which may result in delayed fault estimation.

Model-based methods are further categorized into state estimation and parameter estimation [11]. The former compares the system states estimated by observers with the measured ones. ITSC faults can be identified and located by analyzing and evaluating residual signals. Kalman filter, Luenberger observer and disturbance observer are commonly applied in ITSC fault diagnosis. In [19], both the location and the severity of ITSC faults are estimated through an extended Kalman filter and an unscented Kalman filter. The voltage distortions are estimated by a Luenberger observer in [20]. The fault characteristic signal is constructed in terms of the second harmonic component for ITSC fault diagnosis. In [21], a fault diagnosis method based on a disturbance observer is proposed by using the obtained disturbance signals. However, the above-mentioned research predominantly estimate the integration of short-circuit current and short-circuit turn ratio without achieving decoupling. Meanwhile, the estimation of

Manuscript received April 19, 2025; revised May 14, 2025; accepted June 09, 2025. Date of publication June 25, 2025; Date of current version June 18, 2025.

This work was supported in part by the National Natural Science Foundation of China under Grant 52307056 and in part by the Natural Science Foundation of Jiangsu Province under Grant BK20210475.

Y. J. Huang, W. T. Huang, and T. L. Pan are with the School of Internet of Things Engineering, Jiangnan University, Wuxi 214122, China (e-mail: h1224yj@163.com; wentao.h@jiangnan.edu.cn; tlpan@jiangnan.edu.cn).

D. Z. Xu is with the School of Electrical Engineering, Southeast University, Nanjing 210096, China (e-mail: xudezhi@seu.edu.cn).

(Corresponding Author: Wentao Huang)

Digital Object Identifier 10.30941/CESTEMS.2025.00019

short-circuit resistance remains unaddressed [20]-[22]. Parameter estimation facilitates fault diagnosis by comparing the estimated critical parameters under fault conditions with the values under normal states. A dual-signature diagnostic framework with dynamic bandwidth synchronization for dual-loop regulated systems is established in [23]. The second harmonic ratio in the DC bus voltage is defined as the first fault indicator when only the bandwidth variation of the current controller is considered. The second indicator ensures robustness and enhances ITSC detection accuracy under variations of current and voltage controller bandwidths by weighting and summing the second harmonic components from the DC bus voltage, q-axis current and voltage. In comparison, state estimation methods exhibit lower dependency on precise motor parameters while demonstrating enhanced adaptability to system variations, thus offering superior reliability in dynamic operating conditions. Nevertheless, parameter estimation methods face limitations in fault diagnosis due to the susceptibility to motor parameter variations.

Very recently, fault diagnosis methods based on AI have attracted extensive attention due to their superior learning abilities, effective data processing and robust generalization performance [24]-[26]. In motor fault diagnostics, three deep learning models demonstrate superior performance: convolutional neural networks (CNNs), residual neural networks, and conditional generative adversarial networks (CGANs). In [6], a multi-scale convolutional residual network incorporating dual attention mechanisms for ITSC fault diagnosis is developed, where a spatial attention residual module is strategically integrated to strengthen discriminative feature extraction while counteracting gradient dissipation. To alleviate the heavy reliance on extensive datasets, CGAN is developed based on CNN to expand and collect datasets in [26], and then a deep Q-network (DQN) -driven diagnostic architecture is implemented. In contrast to signal-based and model-based methods, AI-based methods avoid the need for precise mathematical models, enable automatic feature extraction for analysis and prediction, and demonstrate superior diagnostic efficiency with enhanced robustness.

Since observers require only minimal fault information while AI excels in handling nonlinear and u N modeled dynamic systems, this article proposes an ITSC fault diagnosis method that combines an extended state observer (ESO) and a CNN for five-phase PMSMs. Through analyzing the relationship between short-circuit current and fault parameters, a fault diagnosis index is accordingly derived based on the established short-circuit model. Subsequently, an ESO is designed to achieve real-time observation of the diagnostic index, enabling online detection and location of the ITSC fault. By implementing a sensitivity analysis, five fault indicators are selected as the input of the CNN to estimate the short-circuit turn ratio. Therefore, short-circuit current and resistance are decoupled based on the obtained short-circuit turn ratio. As a result, the proposed method enables the estimation of short-circuit current, turn ratio, and resistance, achieving real-time quantitative assessment of fault severity.

II. ITSC FAULT MODEL OF FIVE-PHASE PMSM

A. Mathematical Model

The equivalent circuit model with an ITSC fault in phase-A of a five-phase PMSM is shown in Fig. 1. Assuming that the total turns number of each phase winding is N with N_f representing the number of short-circuit turns, establishing the short-circuit turn ratio $\mu = N_f/N$. The insulation degradation level is quantified by the fault resistance R_f , while i_f is defined as the short-circuit current. R_s and L_s are the phase resistance and phase inductance. The back electromotive force (EMF) for each phase is denoted by e_x ($x = a, b, c, d, e$).

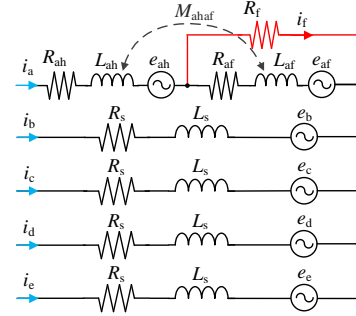


Fig. 1. Equivalent circuit model with ITSC fault in a five-phase PMSM.

Due to the short-circuit fault, the phase-A winding is divided into short-circuited turns and unfaulty turns. R_{ah} , L_{ah} , and e_{ah} are the resistance, inductance, and back EMF of the healthy turns, whereas R_{af} , L_{af} , and e_{af} represent those of the short-circuited turns, respectively [21]. M_{ahaf} is the mutual inductance between the healthy turns and the faulty turns of phase-A winding. According to the relationship between resistance, inductance, back EMF and the short-circuit turn ratio, the following expressions can be derived as:

$$\begin{cases} R_{ah} = (1-\mu)R_s, & R_{af} = \mu R_s \\ L_{ah} = (1-\mu)^2 L_s, & L_{af} = \mu^2 L_s \\ e_{ah} = (1-\mu)e_a, & e_{af} = \mu e_a \end{cases} \quad (1)$$

The ITSC failure is simulated by injecting a short-circuit current i_f into a specific winding. The equivalent circuit model under the ITSC fault condition is considered an extension of the normal five-phase PMSM model. Neglecting nonlinear factors and magnetic saturation and the mutual inductance between the faulty phase and other phases, the voltage of a five-phase PMSM under ITSC faults can be deduced as:

$$\begin{bmatrix} u_a \\ u_b \\ u_c \\ u_d \\ u_e \end{bmatrix} = \begin{bmatrix} R_s & 0 & 0 & 0 & 0 \\ 0 & R_s & 0 & 0 & 0 \\ 0 & 0 & R_s & 0 & 0 \\ 0 & 0 & 0 & R_s & 0 \\ 0 & 0 & 0 & 0 & R_s \end{bmatrix} \begin{bmatrix} i_a \\ i_b \\ i_c \\ i_d \\ i_e \end{bmatrix} + \begin{bmatrix} e_a \\ e_b \\ e_c \\ e_d \\ e_e \end{bmatrix} - \mu R_s \begin{bmatrix} i_f \\ 0 \\ 0 \\ 0 \\ 0 \end{bmatrix} + \begin{bmatrix} L_s & 0 & 0 & 0 & 0 \\ 0 & L_s & 0 & 0 & 0 \\ 0 & 0 & L_s & 0 & 0 \\ 0 & 0 & 0 & L_s & 0 \\ 0 & 0 & 0 & 0 & L_s \end{bmatrix} \begin{bmatrix} di_a/dt \\ di_b/dt \\ di_c/dt \\ di_d/dt \\ di_e/dt \end{bmatrix} - \mu L_s \begin{bmatrix} di_f/dt \\ 0 \\ 0 \\ 0 \\ 0 \end{bmatrix} \quad (2)$$

where u_x ($x = a, b, c, d, e$) and i_x ($x = a, b, c, d, e$) indicate phase voltage and current, respectively.

Neglecting the reluctance torque, the output torque under ITSC fault is given as:

$$T_{ef} = -\frac{e_a i_a + e_b i_b + e_c i_c + e_d i_d + e_e i_e - e_{af} i_f}{\omega_m} \quad (3)$$

where ω_m is the mechanical angular velocity.

B. Short-circuit Current Analysis

According to (2), the voltage of the short-circuit loop is obtained as:

$$L_{af} \frac{di_f}{dt} + (R_{af} + R_f) i_f - i_a R_{af} + \mu L_s \frac{di_a}{dt} - e_{af} = 0 \quad (4)$$

The equation above can be regarded as a first-order nonhomogeneous linear differential equation with constant coefficients. Hence, the short-circuit current is calculated as:

$$\bar{i}_f = \frac{\bar{i}_a (R_s + j\omega_e L_s) + \bar{e}_a}{\left(\frac{R_f + R_s}{\mu} \right) + j\omega_e \mu L_s} \quad (5)$$

where ω_e is the electrical angular velocity.

As presented in (5), R_s and L_s are motor parameters. When a motor operates in steady-state conditions, the electrical angular velocity, amplitudes of phase currents, and back EMFs remain constant. Therefore, the magnitude of the short-circuit current exhibits strong parametric dependence on both short-circuit resistance R_f and the short-circuit turn ratio μ . In the faulty circuit, the thermal effect generated by the circulating current may accelerate insulation damage and even cause phase-to-phase short-circuit faults. Hence, the real-time monitoring of short-circuit current is crucial for accurate fault diagnosis. However, short-circuit current is closely related to speed and load, and its amplitude and frequency are sensitive to variations in operating points. To precisely assess the severity of ITSC faults, the short-circuit turn ratio is regarded as the characteristic indicator of fault severity in this paper. Nevertheless, this variable is typically treated as an unknown parameter due to challenges in direct measurement [10]-[15].

III. PROPOSED FAULT DIAGNOSIS AND SEVERITY ESTIMATION

To achieve the diagnosis and severity estimation of ITSC faults in five-phase PMSMs, this paper develops a fault parameter identification method based on ESO and CNN, the structure of which is illustrated in Fig. 2. The fault diagnosis module consists of observation and identification components. Firstly, the ESO is designed to observe the integration of the short-circuit turn ratio and the current for fault detection and location. Secondly, the CNN is utilized to further estimate the short-circuit turn ratio, thereby assessing the fault severity. The control strategy adopts model predictive current control, which has been extensively applied in multi-phase motor fields due to its simple structure and effective handling of harmonic constraints [27]-[28].

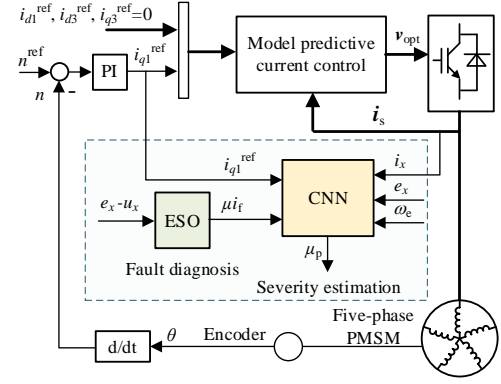


Fig. 2. System control structure and diagnostic algorithm.

A. Parameters Design and Stability Analysis

Combining (2) and (3), the fault diagnosis index μi_f can be expressed as:

$$\frac{d\mu i_f}{dt} = \frac{-R_s \mu i_f + L_s \frac{di_x}{dt} + R_s i_x + e_x - u_x}{L_s} \quad (6)$$

For the convenience of observation, $e_x - u_x$ is taken as the input $u(t)$ of the observer. Thus, the time-domain differential equation based on (6) can be formulated as:

$$\dot{x}_f(t) = Eu(t) + F(t) \quad (7)$$

where $F(t) = \frac{-R_s \mu i_f + L_s \frac{di_x}{dt} + R_s i_x}{L_s}$, x_f represents μi_f , E is the input gain and $F(t)$ is the remaining term.

According to (7), a linear ESO with state variables x_f and F can be constructed as:

$$\begin{cases} \dot{e}_{\tau} = z_1 - x_f \\ \dot{z}_1 = z_2 + Eu - \beta_1 e_{\tau} \\ \dot{z}_2 = -\beta_2 e_{\tau} \end{cases} \quad (8)$$

where $z_1 = \hat{x}_f$ and $z_2 = \hat{F}$ represent the estimated value of x_f and F . e_{τ} is the estimation error, β_1 and β_2 are the error feedback gains of ESO. The structure of ESO is illustrated in Fig. 3.

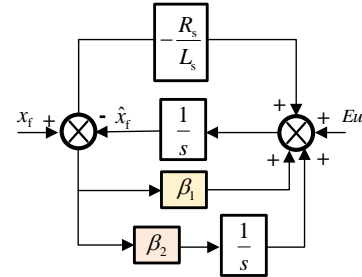


Fig. 3. Structure of ESO.

In this method, the error feedback gain determines the estimation accuracy of the ESO, thus the design of β_1 and β_2 is crucial. By rewriting (8) in matrix form, it can be represented as:

$$\begin{cases} \dot{z} = Az + Bu + D(y - \hat{y}) \\ \hat{y} = Cz \end{cases} \quad (9)$$

where \hat{y} represents the estimated value of y , $A = \begin{bmatrix} 0 & 1 \\ 0 & 0 \end{bmatrix}$,

$$B = \begin{bmatrix} E \\ 0 \end{bmatrix}, C = [1 \ 0], D = \begin{bmatrix} \beta_1 \\ \beta_2 \end{bmatrix}, z = \begin{bmatrix} z_1 \\ z_2 \end{bmatrix}.$$

Based on (9), the characteristic equation of ESO is given as:

$$|sI - (A - DC)| = s^2 + \beta_1 s + \beta_2 \quad (10)$$

where I represents the identity matrix, and s is the characteristic root of the system. To ensure that all characteristic roots are negative and that there is only one adjustment parameter ω_0 , the observation gains are set as $\beta_1 = 2\omega_0$ and $\beta_2 = \omega_0^2$. ω_0 is the bandwidth of ESO. Generally, if ω_0 is too small (z_1 and z_2 are close to 1), the dynamic performance of the observer deteriorates. Conversely, if ω_0 is too large (z_1 and z_2 are close to 0), it may degrade the system's stability margins and induce closed-loop instability [29].

Through ESO, the integration of the short-circuit current and turn ratio can be observed, achieving the diagnosis of ITSC faults. To decouple these two variables and calculate the short-circuit resistance, this paper further designs a parameter estimation algorithm based on a convolutional neural network.

B. Estimation of Fault Parameters based on CNN

The short-circuit turn ratio serves as an evaluation index for fault severity. To accurately estimate the short-circuit turn ratio, the parameters associated with ITSC faults and easily measured are chosen as training inputs for the CNN. Subsequently, data under various operating conditions are collected, improving the accuracy of estimation. Through the estimated short-circuit turn ratio, the fault severity is evaluated, enabling the estimation of the short-circuit current and the short-circuit resistance separately.

1) Convolutional Layers

CNNs, a prominent deep learning architecture, have been extensively utilized across engineering domains including machine vision, time-series analysis, and multidimensional signal interpretation. It mainly consists of five layers: the input layer for raw data ingestion, the convolutional layer performs localized feature abstraction through kernel operations, the pooling layer executes spatial dimensions via nonlinear compression, the fully connected layer synthesizes hierarchical representations and the output layer makes decisions based on the integrated features. Fig. 4 illustrates the schematic structure of a CNN.

Assuming the input and output of the CNN are X and Y . Their functional correspondence is mathematically characterized by:

$$Y = F(X | \Theta) = f_3(f_2(f_1(X | \theta_1) | \theta_2)) | \theta_3 \quad (11)$$

where $f_i(X|\theta_i)$ ($i = 1, 2, 3$) represent the calculation process of the convolutional layer, pooling layer and fully connected layer, respectively. Θ represents the set of parameters θ . Therefore, the essence of CNN is to extract and transform features of input data through a series of hierarchical

structures and then achieve dimensionality reduction.

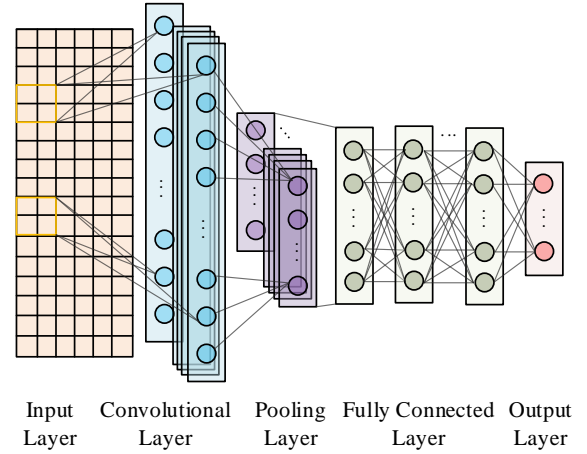


Fig. 4. Architecture of a CNN.

2) Sensitivity Analysis

According to (5) and (6), the short-circuit turn ratio constitutes a complex function of multiple variables including motor parameters, system input and output signals, and short-circuit parameters. Therefore, it is essential to select variables that predominantly affect the short-circuit turn ratio. Therefore, a one-dimensional CNN is used to establish a mapping relationship between the fault indicators and the short-circuit turn ratio μ . The selection process for fault indicators is as follows.

1) The short-circuit current is a characteristic variable that fundamentally characterizes ITSC failure severity, yet its diagnostic utility is constrained by inseparable coupling fault parameters. Consequently, the obtained fault diagnosis index μ_{i_f} through ESO is adopted as the first indicator.

2) Considering the ITSC fault is set in phase-A, parameters such as current, back electromotive force, and voltage of this phase exhibit significant variations. In most of the research on fault diagnosis, current and back EMF are usually regarded as the diagnostic features. Therefore, the faulty phase current i_a and back EMF e_a are selected as the second indicator and the third indicator.

3) Furthermore, the ITSC fault can also cause an elevation of torque ripple. The amplitude and frequency of the torque ripple are related to the load and the electrical frequency, respectively. Therefore, the q_1 -axis current reference i_{q1}^{ref} associated with the torque and the electrical angular velocity ω_e are selected as the fourth indicator and the fifth indicator.

3) Fault Severity Estimation Process

The fault severity estimation process for ITSC is illustrated in Fig. 5, with the specific operational steps as follows.

1) Data processing: To extract the characteristic signals of fault indicators, the FFT is used to calculate the real-time amplitude of the selected fault indicators. To mitigate the influence of varying operating conditions on estimation accuracy, the data is normalized. The ratios of the amplitudes calculated under fault conditions to the steady-state values under normal operation are adopted as sample data.

2) Constructing and training CNN: Configure network parameters such as the learning rate, maximum number of

iterations, number of convolutional layers, etc. Input training and test samples, and update the network parameters through convolution, pooling, activation, and regression operations. Finally, obtain the trained CNN model for online estimation of short-circuit turn ratio μ .

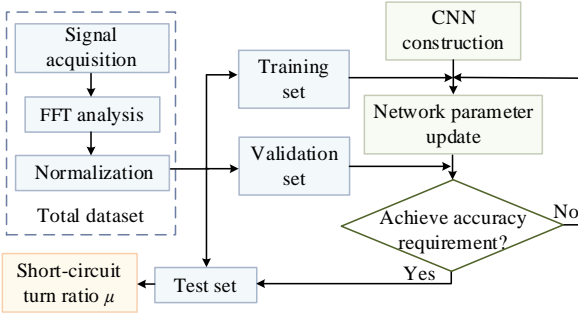


Fig. 5. Fault severity estimation process based on CNN.

IV. SIMULATION VERIFICATION

For validation of the proposed ITSC fault diagnosis method and severity estimation in this article, the ITSC fault model of the five-phase PMSM has been built in Matlab/Simulink. The parameters of the five-phase PMSM are presented in Table I. The sampling frequency of the simulation is 500 kHz, with the current loop bandwidth set to 20 kHz. To enhance disturbance rejection capability, the ESO bandwidth is adjusted to be higher than that of the current loop, thereby producing an angular bandwidth $\omega_0=40200\pi$ rad/s and gains $\beta_1=80400\pi$, $\beta_2=(40200\pi)^2$.

TABLE I
PARAMETERS OF THE FIVE-PHASE PMSM

Parameter	Symbol	Value
Rated speed/(r/min)	n	600
Rated torque/(N·m)	T_{em}	17
Rated phase current/A	I_n	4
Permanent magnet flux-linkage/Wb	ψ_f	0.035
Stator resistance/ Ω	R_s	0.15
d1-axis inductance/mH	L_{d1}	2.5
q1-axis inductance/mH	L_{q1}	2.9
d3-axis inductance/mH	L_{d3}	2.5
q3-axis inductance/mH	L_{q3}	2.5
Number of pole pairs	p_r	18

A. Fault Diagnosis of ITSC

Simulation results are depicted in Fig. 6. The five-phase PMSM operates stably with a speed of 500 r/min and a load of 5 N·m. An ITSC fault occurs at the time instant of 0.07 s. The short-circuit turn ratio is set as 0.3, while the short-circuit resistance is set as 0.2 Ω .

In Fig. 6, the phase currents become unbalanced under the ITSC fault. The total harmonic distortion (THD) of the phase-A current increases from 5.16% to 9.14%, and the torque ripple increases from 2.20% to 46.33%. The observed waveforms of the fault diagnosis index are presented in Fig. 6(c). It can be seen that when the ITSC fault occurs, the amplitude of the fault diagnosis index μ_{if} increases from 0 to

9.66 A with a frequency of 150 Hz. The observed value is consistent with the actual value, demonstrating that the ESO can precisely identify the fault diagnosis index. With the obtained diagnosis index μ_{if} , the ITSC fault can be diagnosed and located.

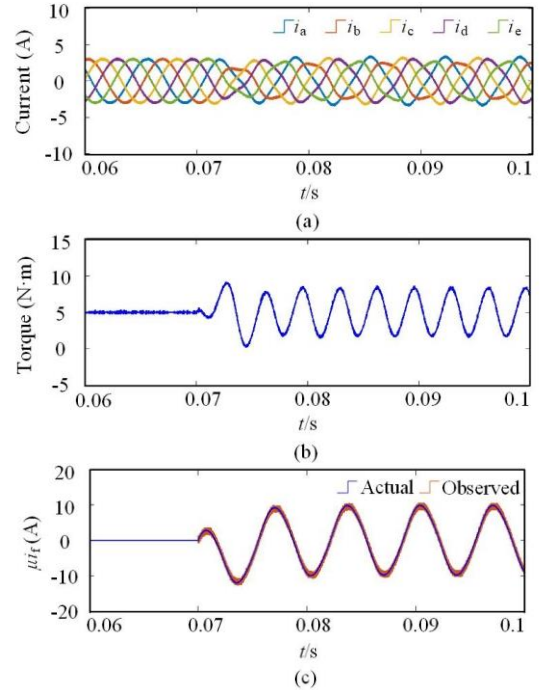


Fig. 6. Simulated waveforms by the proposed diagnostic method. (a) Phase currents. (b) Torque. (c) Fault diagnosis index.

B. Performance of Severity Estimation

To verify the accuracy of CNN in estimating the short-circuit turn ratio, the data under the following four operating points is collected: 1) 450 r/min and 5 N·m, 2) 450 r/min and 7 N·m, 3) 500 r/min and 5 N·m, and 4) 500 r/min and 7 N·m.

The short-circuit turn ratio μ varies from 0.300 to 0.890 with an interval of 0.01. A total of 240 training sample sets are collected from the operating conditions mentioned above and partitioned into 168 training sets (70%), 36 validation sets (15%) and 36 test sets (15%).

The short-circuit resistance is maintained at a fixed value of 0.2 Ω , and the short-circuit turn ratio is set to 0.5 and 0.8. The absolute values of the deviations between the estimated values and the actual values are presented in Table II. The results show that the trained CNN model can well estimate the short-circuit turn ratio with a deviation of less than 0.002 and the average accuracy is 99.48%, verifying that the proposed method is effective.

According to the short-circuit turn ratio estimated by CNN, the short-circuit current i_f can be further deduced. As demonstrated in Fig. 7, the waveform before $t=0.16$ s is the fault diagnosis index μ_{if} and the waveform after $t=0.16$ s is the estimated short-circuit current i_{fp} . Thus, the fault characteristic μ_{if} can be decomposed into two independent parts: short-circuit turn ratio and short-circuit current. Fig. 7(a) presents the influence of different short-circuit turn ratios on the amplitude of the short-circuit current when the short-circuit

resistance is specified as 0.2Ω . It can be observed that as the short-circuit turn ratio increases, the amplitude of i_{fp} shows a decreasing trend, being 35.97 A, 23.09 A and 16.66 A, respectively. Fig. 7(b) shows the influence of different short-circuit resistances on the amplitude of the short-circuit current when the short-circuit turn ratio is fixed at 0.5. As the short-circuit resistance increases, the amplitude of the short-circuit current shows an increasing trend, which is 18.01 A, 23.09 A and 30.17 A, respectively.

TABLE II
ESTIMATION ERRORS OF TURN RATIOS UNDER DIFFERENT OPERATING CONDITIONS

Actual value	Condition	Average value	Error
0.500	450 r/min, 5 N m	0.499	0.001
	450 r/min, 7 N m	0.500	0
	500 r/min, 5 N m	0.499	0.001
	500 r/min, 7 N m	0.501	0.001
	450 r/min, 5 N m	0.800	0
0.800	450 r/min, 7 N m	0.798	0.002
	500 r/min, 5 N m	0.800	0
	500 r/min, 7 N m	0.801	0.001

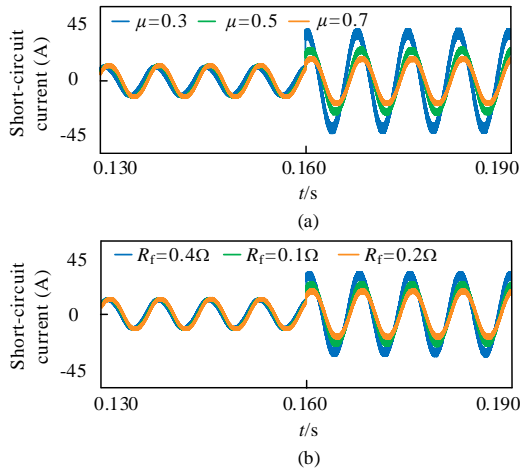


Fig. 7. Short-circuit current under different fault parameters. (a) Short-circuit turn ratio variation. (b) Short-circuit resistance variation.

However, the relationship among short-circuit current, resistance and turn ratio is not monotonically increasing or decreasing [30]. In some cases, an increase in the short-circuit resistance or short-circuit turn ratio may lead to an increase in the short-circuit current, while in other cases, the opposite phenomenon may occur. It may be due to the asymmetry of motor parameters owing to ITSC faults, which results in a more complex electromagnetic field distribution. Besides, the nonlinear issues in motor drives, such as saturation effects and hysteresis effects, and operation conditions would also affect the relationship.

In summary, it can be concluded that both the short-circuit resistance and the short-circuit turn ratio are important factors affecting the short-circuit current. To more comprehensively analyze the trend of the short-circuit current, both the short-circuit resistance and the short-circuit turn ratio need to be taken into account.

Given the known short-circuit turn ratio and short-circuit

current, (5) can be written as:

$$|i_f| = \frac{\mu \lambda_{pm} \omega_c}{\sqrt{(R_f + \mu R_a)^2 + (\omega_c \mu^2 L_a)^2}} \quad (12)$$

where λ_{pm} is the amplitude of the permanent magnet flux linkage.

In Fig. 8, the short-circuit resistance R_f is calculated using (12) in real-time. The speed is set to 500 r/min with a constant load of 5 N m. A short-circuit fault occurs at 0.07 s and the short-circuit turn ratio μ is set as 0.3.

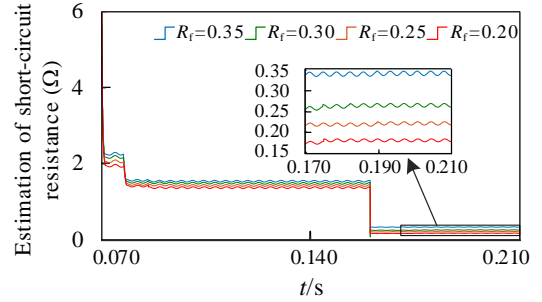


Fig. 8. Online calculation of short-circuit resistance.

When the short-circuit resistances are 0.20Ω , 0.25Ω , 0.30Ω , and 0.35Ω , the calculated short-circuit resistances R_{fc} are 0.18Ω , 0.22Ω , 0.27Ω , and 0.35Ω respectively. The results indicate that the calculated R_{fc} match the actual values satisfactorily with a deviation of less than 0.02 and the average accuracy is 92%.

V. EXPERIMENTS

To further prove the diagnostic capability of the proposed method, StarSim MT3200 test platform is used to conduct real-time simulation experiments. Fig. 9 depicts the experimental setup, which includes the host computer, StarSim MT3200 and dSPACE1202. The five-phase voltage source inverter circuit is constructed through a real-time hardware-in-loop system. The control algorithm and five-phase PMSM model are completed by dSPACE1202. The sampling frequency used in the experimental test is 50 kHz. The real-time simulator and controller are connected through actual physical I/O, which transmits signals. The parameters of the PMSM are consistent with those used in the simulations. The short-circuit turn ratio is set as 0.8 and the short-circuit resistance is set as 0.2Ω .

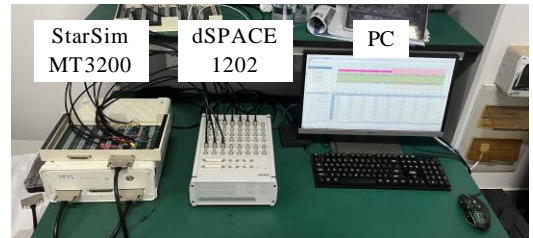


Fig. 9. Experimental setup.

A. Performance under Operating Points Variation

Two tests are conducted to validate the diagnostic method

against operating point variations. The dynamic results under speed and load variations are respectively captured in Fig. 10 and Fig. 11. As illustrated in Fig. 10, the five-phase drive system operates at a speed of 300 r/min and a load of 17 N m under healthy and ITSC situations. After the occurrence of an ITSC fault, all phase currents are amplified to different degrees. The THD of phase-A current increases from 8.37% to 9.24%, as listed in Table III. Meanwhile, the torque ripple escalates significantly, increasing from 2.04% to 24.17%. Fig. 11 demonstrates the five-phase PMSM operates with a constant speed of 550 r/min and a 15 N m load. Upon the appearance of a short-circuit fault, the current THD in phase-A increases from 10.44% to 11.09%, and the torque ripple increases from 4.01% to 23.42%.

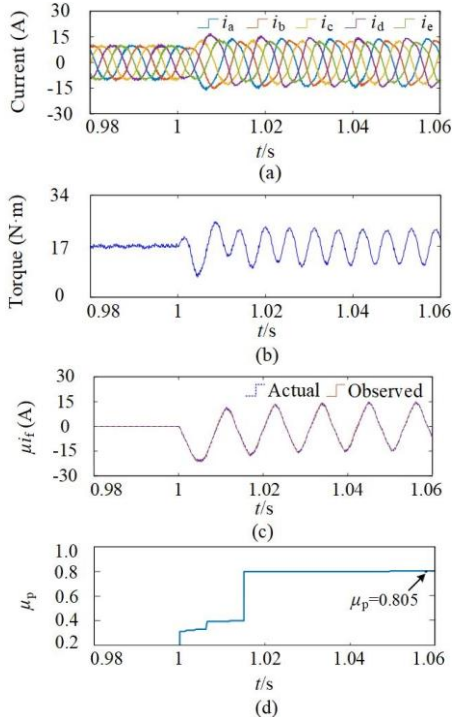


Fig. 10. Experimental waveforms under normal and faulty conditions at 17 N m and 300 r/min. (a) Phase currents. (b) Torque. (c) Fault diagnosis index. (d) Estimated short-circuit turn ratio.

TABLE III

THD VALUES OF PHASE-A CURRENT AND TORQUE RIPPLE UNDER NORMAL AND FAULT CONDITIONS

Operating point	Condition	THD of phase-A current (%)	Torque ripple (%)
$n=300$ r/min	Normal	8.37	2.04
$T_l=17$ N m	$R_f=0.2 \Omega, \mu=0.8$	9.24	24.17
$n=550$ r/min	Normal	10.44	4.01
$T_l=15$ N m	$R_f=0.2 \Omega, \mu=0.8$	11.09	23.42

As demonstrated in Fig. 10(c) and Fig. 11(c), the observed fault diagnosis index can track the actual value. Upon ITSC fault occurrence, the amplitude of the fault diagnosis index μ_{if} rapidly increases to 15 A. Fig. 10(d) and Fig. 11(d) show the real-time estimation of the short-circuit turn ratio. The results demonstrate that the estimated value rapidly approaches the actual value within 0.02 s. The estimated values of the short-circuit turn ratio μ_p obtained are 0.805 and 0.798, respectively.

It is concluded that this method can quickly and accurately estimate the short-circuit turn ratio under the ITSC fault condition inferred from the input signals, achieving the severity estimation of the ITSC fault.

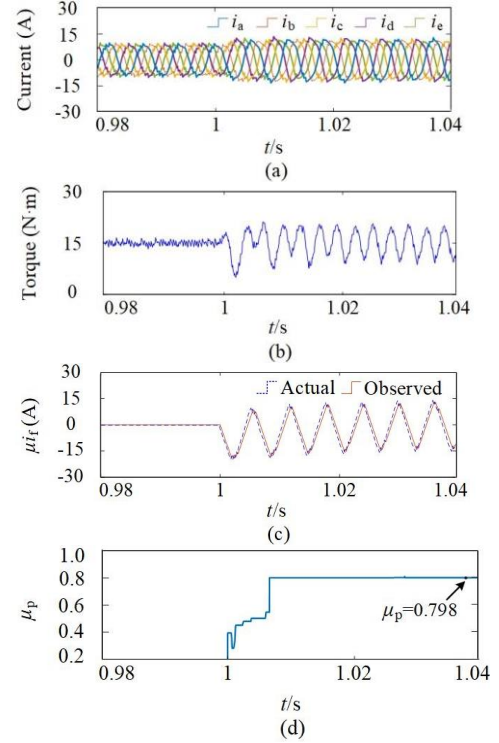


Fig. 11. Experimental waveforms under normal and faulty conditions at 15 N m and 550 r/min. (a) Phase currents. (b) Torque. (c) Fault diagnosis index. (d) Estimated short-circuit turn ratio.

B. Dynamic Performance

To validate the robustness of the proposed method, experiments are implemented under conditions of varying speeds and loads. Fig. 12 presents experimental results of the speed change from 300 r/min to 500 r/min with a constant load of 15 N m. As the ITSC fault occurs, the amplitude of the diagnosis indicator demonstrates a rapid surge to 15 A, with observed values closely tracking actual measurements. Besides, the estimated short-circuited turn ratio stabilizes at 0.397 after a transient fluctuation. The mean deviation between predicted values and the actual reference value of 0.400 remains within 0.008, indicating stable diagnostic performance under dynamic operational conditions.

The experimental waveforms of the load stepping from 8 N m to 16 N m with a constant speed of 300 r/min are illustrated in Fig. 13. Post-load variation results reveal the amplitude increase in both phase currents and the diagnostic indicator. Simultaneously, the fault diagnosis index observed demonstrates precise tracking performance throughout the load variation. Furthermore, estimation results of the short-circuit turn ratio remain consistent, exhibiting a deviation of 0.004 from the actual value of 0.700.

In conclusion, the experimental results verify the robustness of the proposed method, demonstrating sustained diagnostic stability and achieving an average fault evaluation accuracy rate of 98.84% under dynamic operational conditions.

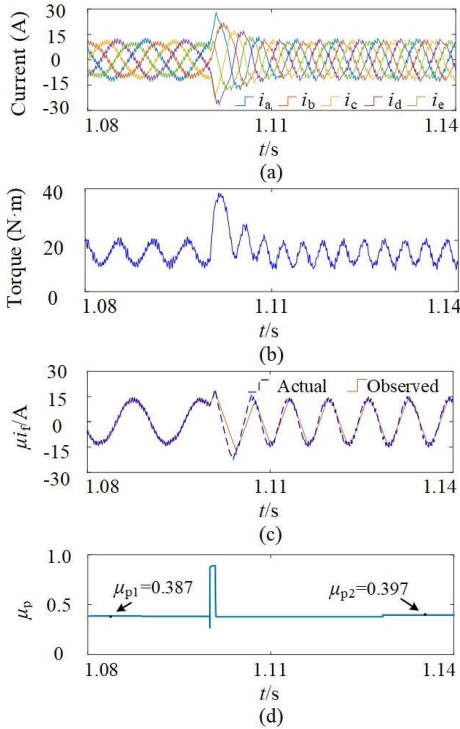


Fig. 12. Experimental waveforms under speed variation. (a) Phase currents. (b) Torque. (c) Fault diagnosis index. (d) Estimated short-circuit turn ratio.

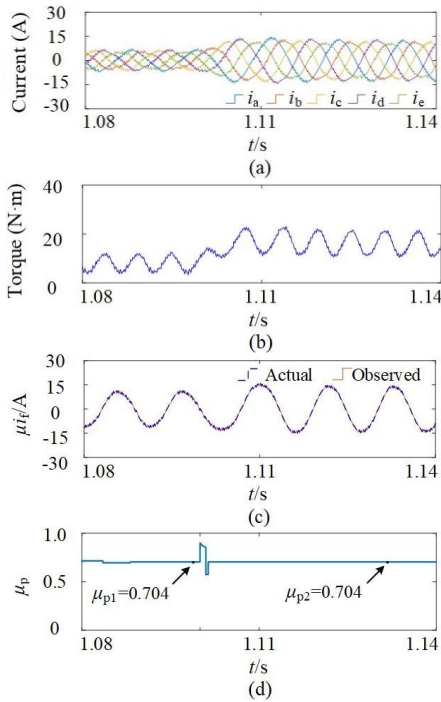


Fig. 13. Experimental waveforms under torque variation. (a) Phase currents. (b) Torque. (c) Fault diagnosis index. (d) Estimated short-circuit turn ratio.

C. Estimation Results

To assess the estimation algorithm's accuracy of the estimated short-circuit turn ratio across operational differences, the short-circuit turn ratio varied within the range from 0.300 to 0.850 with an interval of 0.050. Fig. 14 depicts the estimation results of the short-circuit turn ratios. The absolute value of the largest deviation is 0.036 while the

others are less than 0.013, which demonstrates that the estimation method of short-circuit turn ratio under different operating conditions is effective.

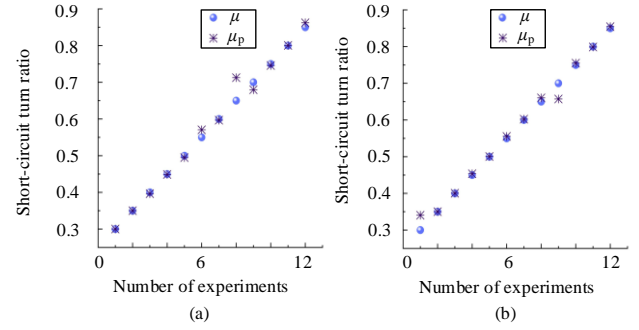


Fig. 14. Estimation results under different fault severities. (a) At 300 r/min and 17 N·m. (b) At 550 r/min and 15 N·m.

The comprehensive analysis results indicate that the ESO can effectively detect and localize ITSC faults by estimating the integration of the short-circuit current and the short-circuit turn ratio. Moreover, online estimation results under different operating points and fault severities demonstrate that the CNN enables rapid quantification of fault severity. Table IV provides a comprehensive comparison between the proposed method and existing diagnostic approaches, evaluating three aspects: fault localization, evaluation of fault severity, and fault parameter decoupling. The results demonstrate that the developed algorithm exhibits significant performance advantages in fault identification, whereas other methods exhibit one or more limitations.

TABLE IV
COMPARISONS WITH EXISTING WORK

Method	Fault location	Severity evaluation	Fault parameters decoupling
Method based on voltage distortion [20]	Yes	No	No
Method based on a disturbance observer [21]	No	No	No
Method based on current and voltage controllers [23]	No	No	No
Method based on decision-making framework [24]	Yes	Yes	No
Proposed method	Yes	Yes	Yes

VI. CONCLUSION

This article proposed an ITSC fault diagnosis and severity estimation method for five-phase PMSM drives. The short-circuit current is analytically modeled based on the developed equivalent circuit model. The real-time observation of the fault diagnosis index through an ESO enables online fault detection and location. Through sensitivity analysis of faults and motor parameters, five fault indicators are selected and collected under diverse operating conditions. Subsequently, A CNN model is trained to estimate the short-circuit turn ratio, enabling a quantitative assessment of fault severity. Furthermore, the inherent coupling between fault parameters is resolved. The operational reliability and diagnostic accuracy of the developed method are validated through simulations and experiments under diverse load conditions.

REFERENCES

- [1] W. T. Huang, X. F. Zhu, and H. L. Zhang *et al.*, "Generalized Fault-tolerant Model Predictive Control of Five-phase PMSM Drives under Single/Two Open-switch Faults," *IEEE Transactions on Industrial Electronics*, vol. 70, no. 8, pp. 7569–7579, Aug. 2023.
- [2] W. Hua, F. Y. Chen, and W. T. Huang *et al.*, "Multivector-based Model Predictive Control with Geometric Solution of a Five-phase Flux-switching Permanent Magnet Motor," *IEEE Transactions on Industrial Electronics*, vol. 67, no. 12, pp. 10035–10045, Dec. 2020.
- [3] S. Sonandkar, R. Selvaraj, and T. Raj Chelliah, "PV Powered Improved Quasi-z-source Inverter Fed Five Phase PMSM for Marine Propulsion Systems," *IEEE Transactions on Transportation Electrification*, vol. 11, no. 1, pp. 393–403, Feb. 2025.
- [4] J. Huang, Z. S. Yin, and T. Y. Wang *et al.*, "Diagnosis of Inter-turn Short-circuit Fault for Five-phase Permanent Magnet Machine based on Fault-tolerant Tooth Flux," *Transactions of China Electrotechnical Society*, vol. 38, no. 14, pp. 3733–3744, Jul. 2023.
- [5] Q. Chen, X. Y. Dai, and X. J. Song *et al.*, "ITSC Fault Diagnosis for Five Phase Permanent Magnet Motors by Attention Mechanisms and Multiscale Convolutional Residual Network," *IEEE Transactions on Industrial Electronics*, vol. 71, no. 8, pp. 9737–9746, Aug. 2024.
- [6] Y. Zhao, C. Shen, and D. D. Li *et al.*, "Inter-turn Short Circuit Diagnosis of Wound-field Doubly Salient Machine based on Multi-signal Fusion on Feature Level under Extreme Conditions," *Transactions of China Electrotechnical Society*, vol. 38, no. 10, pp. 2661–2674, May 2023.
- [7] Y. Zhao, J. Y. Lu, and D. D. Li *et al.*, "A Fault Diagnosis Strategy for Winding Inter-turn Short-circuit Fault in Doubly Salient Electromagnetic Machine based on Mechanical and Electrical Signal Fusion," *Transactions of China Electrotechnical Society*, vol. 38, no. 1, pp. 204–219, Jan. 2023.
- [8] P. Chen, Y. Xie, and D. L. Li, "Research on the Temperature Rise Characteristics of Induction Motors with Stator Inter-turn Fault," *Transactions of China Electrotechnical Society*, vol. 38, no. 18, pp. 4875–4888, Sept. 2023.
- [9] F. Parvin, J. Faiz, and Y. Qi *et al.*, "A Comprehensive Interturn Fault Severity Diagnosis Method for Permanent Magnet Synchronous Motors based on Transformer Neural Networks," *IEEE Transactions on Industrial Informatics*, vol. 19, no. 11, pp. 10923–10933, Nov. 2023.
- [10] Y. Qi, E. Bostanci, and M. Zafarani *et al.*, "Severity Estimation of Interturn Short Circuit Fault for PMSM," *IEEE Transactions on Industrial Electronics*, vol. 66, no. 9, pp. 7260–7269, Sept. 2019.
- [11] Y. T. Jiang, B. J. Ji, and J. Zhang *et al.*, "An Overview of Diagnosis Methods of Stator Winding Inter-turn Short Faults in Permanent-magnet Synchronous Motors for Electric Vehicles," *World Electric Vehicle Journal*, vol. 15, no. 4, pp. 165, Apr. 2024.
- [12] R. H. Cui, Y. Fan, and C. X. Li, "On-line Inter-turn Short-circuit Fault Diagnosis and Torque Ripple Minimization Control Strategy based on OW Five-phase BFTHE-IPM," *IEEE Transactions on Energy Conversion*, vol. 33, no. 4, pp. 2200–2209, Dec. 2018.
- [13] J. Hang, W. S. Sun, and Q. T. Hu *et al.*, "Integration of Interturn Fault Diagnosis and Fault-tolerant Control for PMSM Drive System," *IEEE Transactions on Transportation Electrification*, vol. 8, no. 2, pp. 2825–2835, Jun. 2022.
- [14] C. Y. Wu, C. Q. Guo, and Z. W. Xie *et al.*, "A Signal-based Fault Detection and Tolerance Control Method of Current Sensor for PMSM Drive," *IEEE Transactions on Industrial Electronics*, vol. 65, no. 12, pp. 9646–9657, Dec. 2018.
- [15] M. Zafarani, E. Bostanci, and Y. Qi *et al.*, "Interturn Short-circuit Faults in Permanent Magnet Synchronous Machines: An Extended Review and Comprehensive Analysis," *IEEE Journal of Emerging and Selected Topics in Power Electronics*, vol. 6, no. 4, pp. 2173–2191, Dec. 2018.
- [16] K. H. Kim, "Simple Online Fault Detecting Scheme for Short-circuited Turn in a PMSM Through Current Harmonic Monitoring," *IEEE Transactions on Industrial Electronics*, vol. 58, no. 6, pp. 2565–2568, Jun. 2011.
- [17] P. Pietrzak, and M. Wolkiewicz, "Fault Diagnosis of PMSM Stator Winding based on Continuous Wavelet Transform Analysis of Stator Phase Current Signal and Selected Artificial Intelligence Techniques," *Electronics*, vol. 12, no. 7, pp. 1543, Apr. 2023.
- [18] C. Wang, X. Liu, and Z. Chen, "Incipient Stator Insulation Fault Detection of Permanent Magnet Synchronous Wind Generators based on Hilbert–huang Transformation," *IEEE Transactions on Magnetics*, vol. 50, no. 11, pp. 1–4, Nov. 2014.
- [19] W. El Sayed, M. A. El Geliel, and A. Lotfy, "Fault Diagnosis of PMSG Stator Inter-turn Fault Using Extended Kalman Filter and Unscented Kalman Filter," *Energies*, vol. 13, no. 11, pp. 2972, Jun. 2020.
- [20] J. Hang, Q. T. Hu, and W. S. Sun *et al.*, "A Voltage-distortion-based Method for Robust Detection and Location of Interturn Fault in Permanent Magnet Synchronous Machine," *IEEE Transactions on Power Electronics*, vol. 37, no. 9, pp. 11174–11186, Sept. 2022.
- [21] Q. Chen, X. Han, and G. H. Liu *et al.*, "Inter-turn Fault Diagnosis and Control for Five-phase PMSMs by Disturbance Observer," *IEEE Transactions on Industrial Electronics*, vol. 71, no. 11, pp. 13901–13909, Nov. 2024.
- [22] P. N. Luo, Z. G. Yin, and Z. Zhang *et al.*, "Diversified Diagnosis Strategy for PMSM Inter-turn Short-circuit Fault via Novel Sliding Mode Observer," *IEEE Transactions on Power Electronics*, vol. 39, no. 4, pp. 4149–4159, Apr. 2024.
- [23] F. Niu, W. Feng, and S. P. Huang *et al.*, "Robust Inter-turn Short-circuit Fault Detection in PMSGs with Respect to the Bandwidths of Current and Voltage Controllers," *IEEE Transactions on Power Electronics*, vol. 38, no. 8, pp. 10269–10279, Aug. 2023.
- [24] L. Zezula, M. Kozovsky, and P. Blaha, "Diagnostics of Interturn Short Circuits in PMSMs with Online Fault Indicators Estimation," *IEEE Transactions on Industrial Electronics*, vol. 71, no. 11, pp. 15001–15011, Nov. 2024.
- [25] Y. J. Li, Y. F. Chen, and K. Zhu *et al.*, "An Effective Federated Learning Verification Strategy and Its Applications for Fault Diagnosis in Industrial IOT Systems," *IEEE Internet of Things Journal*, vol. 9, no. 18, pp. 16835–16849, Sept. 2022.
- [26] Y. J. Li, R. Q. Wang, and R. Z. Mao *et al.*, "A Fault Diagnosis Method based on an Improved Deep Q-network For the Interturn Short Circuits of a Permanent Magnet Synchronous Motor," *IEEE Transactions on Transportation Electrification*, vol. 10, no. 2, pp. 3870–3887, Jun. 2024.
- [27] W. T. Huang, W. Hua, and Q. G. Fan, "Performance Analysis and Comparison of Two Fault-tolerant Model Predictive Control Methods for Five-phase PMSM Drives," *CES Transactions on Electrical Machines and Systems*, vol. 5, no. 4, pp. 311–320, Dec. 2021.
- [28] W. T. Huang, M. J. Huang, and W. L. Yang *et al.*, "Continuous-control-set Model-free Predictive Current Control with Voltage Correction of Five-phase PMSM," *IEEE Transactions on Energy Conversion*, Early Access, pp. 1–10, 2025, doi: 10.1109/TEC.2025.3532671.
- [29] Y. C. Zhang, J. L. Jin, and L. L. Huang, "Model-free Predictive Current Control of PMSM Drives based on Extended State Observer Using Ultralocal Model," *IEEE Transactions on Industrial Electronics*, vol. 68, no. 2, pp. 993–1003, Feb. 2021.
- [30] S. P. Huang, A. Aggarwal, and E. G. Strangas *et al.*, "Mitigation of Interturn Short-circuits in IPMSM by Using MTPCC Control Adaptive to Fault Severity," *IEEE Transactions on Power Electronics*, vol. 37, no. 4, pp. 4685–4696, Apr. 2022.



Yijia Huang received the B.S. degree in electrical engineering from the School of Internet of Things Engineering, Jiangnan University, Wuxi, China, in 2023, where she is currently working toward the M.S. degree. Her research interests include multi-phase motor drives and fault diagnosis.



Wentao Huang received the Ph.D. degree in Electrical Engineering from Southeast University, Nanjing, China, in 2020. From January 2018 to January 2019, he was a joint Ph.D. student with the School of Electrical and Data Engineering, University of Technology Sydney, NSW, Australia.

Since 2020, he has been with Jiangnan University, Wuxi, China, where he is currently an Associate Professor with the School of Internet of Things Engineering. His major research interests include permanent magnet machine drives, fault diagnosis and fault-tolerant control.



Tinglong Pan received the Ph.D. degree in power electronics and power drive from the China University of Mining and Technology, Xuzhou, China, in 2004. He is currently a Professor with Jiangnan University, Wuxi, China. His main research interests include microgrid control technology, power conversion

technology, and power drive systems and its intelligent control technology.



Dezhi Xu received the Ph.D. degree in control theory and control engineering from Nanjing University of Aeronautics and Astronautics, China, in 2013.

From 2018 to 2019, he was a Visiting Fellow with the Department of Biomedical Engineering, City University of Hong Kong, Hong Kong. He is currently a Professor with a Young Endowed Chair Honor with the School of Electrical Engineering, Southeast University, Nanjing, China. His research interests include data-driven control, fault diagnosis and fault-tolerant control, multiagent systems and cyber-physical systems, technologies of renewable energy, motor control, and smart grid. He was a Guest Editor for the International Journal of Innovative Computing, Information and Control and the Electric Power. He is a Committee Member of the Association of Energy Internet, and Trusted Control in Chinese Association of Automation (CAA), and the Energy Storage in China Renewable Energy Society (CRES). He was supported by the National Natural Science Fund for Excellent Young Scientists Fund Program in 2022.